Unabsorbed Seyfert 2 galaxies: the case of 'naked' AGN⋆

F. Panessa,[1]† F. J. Carrera,[2] S. Bianchi,[3] A. Corral,[4] F. Gastaldello,[5,6]‡ X. Barcons,[2]
L. Bassani,[7] G. Matt[3] and L. Monaco[8]

[1]*Istituto di Astrofisica Spaziale e Fisica Cosmica (IASF-INAF), via del Fosso del Cavaliere 100, 00133 Roma, Italy*
[2]*Instituto de Física de Cantabria (CSIC-UC), 39005 Santander, Spain*
[3]*Dipartimento di Fisica, Università degli Studi Roma Tre, via della Vasca Navale 84, 00146 Roma, Italy*
[4]*Osservatorio Astronomico di Brera (OAB-INAF), via Brera 28, 20121 Milano, Italy*
[5]*IASF-Milano, INAF, via Bassini 15, Milano 20133, Italy*
[6]*Department of Physics and Astronomy, University of California at Irvine, 4129, Frederick Reines Hall, Irvine, CA 92697-4575, USA*
[7]*Istituto di Astrofisica Spaziale e Fisica Cosmica (IASF-INAF), Via P. Gobetti 101, 40129 Bologna, Italy*
[8]*Universidad de Concepción, Casilla 160-C, Concepción, Chile*

ABSTRACT

Hawkins reported on a class of 'naked' active galactic nuclei (AGN) characterized by strong amplitude optical brightness variability and the complete absence of broad emission lines in the optical spectrum. The variability suggests that the nucleus is seen directly, however the absence of broad lines contradicts the simple formulation of Unified Models for AGN. We present the results of quasi-simultaneous spectroscopic observations with *XMM–Newton* and New Technology Telescope (NTT) (La Silla) of two 'naked' AGN. We confirm the 'naked' nature of Q2131−427 for which no broad emission line components have been detected in the optical spectrum and its X-ray spectrum shows no signs of intrinsic absorption. The optical and X-ray mismatch in this source cannot be ascribed to a high nuclear dust-to-gas ratio and a Compton-thick nature is ruled out on the basis of the high $F_X/F_{[O\,III]}$ ratio. The broad-line region (BLR) may be completely absent in this source, possibly as a consequence of its low Eddington ratio. On the other hand, the optical spectrum of Q2130−431 shows Hα and Hβ broad emission line components, revealing the presence of a BLR. A mild X-ray absorption is expected in intermediate type 1.8 Seyfert galaxies like Q2130−431, however we put a very low upper limit on the column density ($<2 \times 10^{20}$ cm^{-2}), also the low Balmer decrement suggests that the BLR itself does not suffer from reddening. We propose that in this object the BLR is intrinsically weak, making a case of 'true' intermediate Seyfert galaxy. We also report on the X-ray detection of the Abell 3783 galaxy cluster in the *XMM–Newton* field of view of the Q2131−427 observation.

Key words: galaxies: active – galaxies: clusters: general – galaxies: Seyfert – X-rays: galaxies.

1 INTRODUCTION

The Unified Model for Seyfert galaxies predicts that the differences observed between type 1 and type 2 Seyfert galaxies are primarily due to orientation effects (Antonucci 1993). Optical narrow emission lines present in both type 1 and type 2 Seyfert spectra are produced in the narrow-line region (NLR) at >100 pc scale from the nucleus. Optical broad emission lines originate in the broad-line region (BLR) at sub-pc scale. The latter are observed only in type 1 Seyfert's spectra since, in type 2 Seyferts, they are obscured by a molecular torus. Much evidence has been found in favour of this picture, such as the larger amount of absorbing material measured from X-ray observations in Seyfert 2s with respect to Seyfert 1s (Awaki et al. 1991; Risaliti, Maiolino & Salvati 1999).

However, in the last few years the number of cases in which observations do not match with Unified Models is increasing both in the local and in distant Universe. Type 1 active galactic nuclei (AGN) with significant absorption have been found (Fiore et al. 2001; Mateos et al. 2005; Cappi et al. 2006) along with type 2 AGN without X-ray absorption (Pappa et al. 2001; Panessa & Bassani 2002; Barcons, Carrera & Ceballos 2003; Caccianiga et al. 2004; Corral et al. 2005; Wolter et al. 2005; Bianchi et al. 2008; Brightman & Nandra 2008).

Several explanations have been proposed to reconcile the Unified Model paradigm with these pieces of evidence. For instance,

---

Table 1. The 'naked' AGN sample and *XMM–Newton* observation log.

Name	RA	Dec.	z	[O III]/Hβ	δB	Obs. date M1/M2/PN	Exposure (s) M1/M2/PN	Filters M1/M2/PN
(1)	(2)	(3)	(4)	(5)	(6)	(7)	(8)	(9)
Q2130−431	21 33 15.62	−42 54 24	0.266	16.36	1.20	2006-11-13	29997/29774/24431	M/M/M
Q2131−427	21 34 26.49	−42 29 56	0.365	7.43	1.18	2006-11-15	23698/23429/16140	M/M/M

Notes. Column (1): galaxy name; Columns (2)–(3): optical position in epoch J2000; Columns (4): redshift; Column (5): [O III]/Hβ ratio; Column (6): amplitude of the B_J band measured over the period from 1974 to 2002; Column (7): observation date; Column (8): MOS1/MOS2/PN observation exposures; Column (9): MOS1/MOS2/PN filters, M = medium. Columns (1) and (4)–(6) are from Hawkins (2004).

the broad emission lines could fade away in response to a decrease of the continuum emission (Matt, Guainazzi & Maiolino 2003; Guainazzi et al. 2005). Alternatively, the BLR is covered by clumpy and variable obscuring material, as in NGC 4388 where a variation of a factor of 100 in column density has been observed from X-ray observations (Elvis et al. 2004) and in NGC 1365 where a spectral change from Compton thin to Compton thick and back to Compton thin has happened in four days (Risaliti et al. 2007). In the above-mentioned cases, the misleading X-ray and optical behaviour is basically due to non-simultaneity of the observations. Finally, the BLR could be weak or absent and its formation linked to the accretion physics (Williams, Baker & Perry 1999; Nicastro 2000; Nicastro, Martocchia & Matt 2003; Elitzur & Shlosman 2006; Wang & Zhang 2007). Simultaneous optical and X-ray observations have confirmed that NGC 3147 is BLR-free and without X-ray absorption (Bianchi et al. 2008). The strategy of observing the source simultaneously in the two bands has been proved to be fundamental in order to avoid mismatches due to spectral or flux variability of the source at X-rays and optical wavebands.

Hawkins (2004) presented the results from a long-term monitoring of about 800 quasars. Among them, a new class of AGN is reported, i.e. the 'naked' AGN, where the absence of broad emission lines is accompanied by strong optical variability, suggesting that the nucleus is seen directly. Subsequently, *Chandra* snapshot observations of three 'naked' AGN (Q2130−431, Q2131−427 and Q2122−444) by Gliozzi, Sambruna & Foschini (2007) confirmed this hypothesis given the absence of significant absorption in the X-ray spectra, though of low statistics. In this work, we present quasi-simultaneous X-rays and optical spectroscopic observations with *XMM–Newton* and ESO Multi-Mode Instrument (EMMI)/New Technology Telescope (NTT) [La Silla Observatory (LSO), European Southern Observatory (ESO)] of two sources (Q2130−431 and Q2131−427) out of the six 'naked' AGN sample defined in Hawkins (2004) and discuss their nature with respect to Unified Models and recent developments. We also report on the serendipitous detection of the cluster Abell 3783 in Appendix A. In the following, we adopt $H_0 = 70$ km s^{-1} Mpc^{-1}, $\Omega_\Lambda = 0.73$ and $\Omega_m = 0.27$ (Spergel et al. 2003).

2 THE SAMPLE OF 'NAKED' AGN

Hawkins (2004) carried out a yearly photometrical large-scale monitoring programme for AGN over the last 25 yr. The survey was based on a long series of photographic plates from the United Kingdom 1.2m Schmidt Telescope. Candidate AGN were selected from a catalogue of 200 000 objects to perform follow-up spectroscopic study. Optical spectra (obtained in 2002 July) pinpoint a class of objects (six in that sample) which show narrow and weak Hβ emission line, large [O III]λ5007/Hβ ratios typical of type 2 Seyferts

(i.e. [O III]λ5007/H$\beta > 3$; Shuder & Osterbrock 1981) and no sign of broad emission lines.[1] For this class of objects, the difference between the maximum and minimum light in magnitudes in the B_J passband over a period of 25 yr, δB, reveals large amplitude variations normally found only in type 1 objects. Their brightness varied at least by a factor of 3 on a time-scale of 5–10 yr and also on shorter time-scales (see light curves in Hawkins 2004). Two among the brightest sources of the six 'naked' AGN sample have been observed in this work (Q2130−431 and Q2131−427). In particular, Hawkins (2004) also reported on a previous optical observation of Q2131−427, in 1991 with the ESO Faint Object Spectograph and Camera (EFOSC) on the 3.6 m at ESO, when the source was 0.7 mag brighter than in 2002. Its optical spectrum showed no sign of broad emission lines and weak Hβ, basically consistent with the spectrum observed afterward in 2002, apart from some additional flux at the blue end of the continuum. In Table 1, we report the two observed 'naked' AGN, where redshift, [O III]λ5007/Hβ and δB are taken from Hawkins (2004).

3 DATA REDUCTION AND ANALYSIS

3.1 Optical data

Q2130−431 and Q2131−427 were observed at the NTT in La Silla (Chile) in director discretionary time (ID: 278.B-5021) to obtain a quasi-simultaneous observation with the *XMM–Newton* ones. Observations for both sources have been performed on 2006 December 20 with the EMMI with grating 4 and a 1-arcsec slit width. The condition of the night was good (i.e. clear to photometric). The exposure for each spectrum was of 1200 s (airmass 1.70 for Q2130−431 and 1.92 for Q2131−427). The wavelength resolution measured from unblended arc lines was 3 Å, in the range 6000–9000 Å. A standard reduction process was applied using MIDAS and IRAF tasks. The raw data were bias subtracted and corrected for pixel-to-pixel variations (flat-field). Object spectra were extracted and sky subtracted. Wavelength calibrations were carried out by comparison with exposures of He and Ar lamps, with an accuracy of <1 Å. Relative flux calibration was carried out by observations of the spectrophotometric standard star SA95_42 (Oke 1990). We estimate an error on the flux calibration <10 per cent from the standard adjustment during the calibration procedure. Statistical errors were propagated throughout the data reduction process.

The spectral fitting was carried out using the QDP fitting routines via χ^2 minimization. The spectrum has been fitted with a linear component in order to reproduce the continuum which is always almost flat. The line intensities and widths were measured by fitting

---

[1] Note, however, that the broadness of other emission lines, for instance Hα, could not be determined since this line was redshifted out of the optical passband.

Table 2. Measured line parameters for the optical spectrum of Q2130−431 and Q2131−427.

Line	Q2130−431		Q2131−427	
	Flux (10^{-15} cgs)	FWHM (km s^{-1})	Flux (10^{-15} cgs)	FWHM (km s^{-1})
Hβ (narrow)	0.11	320^{+50}_{-30} (426)^a	0.13	590^{+40}_{-60} (830)^a
Hβ (broad)	1.17	9680^{+190}_{-150}	<0.06	4000*
[O III] λ4959	0.40	370^{+30}_{-20}	0.40	970^{+40}_{-50}
[O III] λ5007	1.19	370 (410)^a	1.21	970 (960)^a
Hα (narrow)	0.39	320	0.54	590
Hα (broad)	4.01	9680	<0.25	4000*
[N II] λ6548	0.22	440^{+20}_{-30}	0.24	890^{+60}_{-70}
[N II] λ6583	0.66	440	0.72	890
[S II] λ6716	0.10	320^{+50}_{-30}	-	-
[S II] λ6731	0.10	320	-	-

Notes. Linewidths for [O III], [N II], [S II] doublets and Balmer line components (narrow and broad, respectively) were fitted by tying down the velocity widths to the same value. Parameters with an asterisk (*) were kept fixed to the reported value during the fitting procedure.
^{a}FWHM in km s^{-1} obtained from Hawkins (2004) after correction for the spectral resolution of 520 km s^{-1} (see Hawkins 2004, section 2.2).
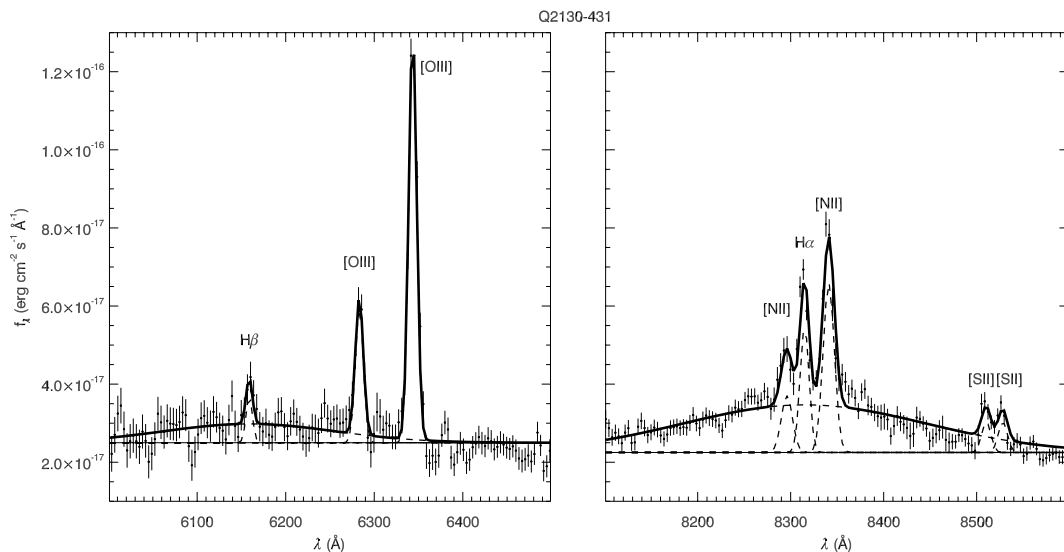
Figure 1. Q2130−431 EMMI optical spectrum. Best-fitting models of the Hβ (left-hand panel) and Hα (right-hand panel) spectral regions.

Gaussian profiles and the full width at half-maximum (FWHM) calculated taking into account the spectrograph resolution. The NLR is stratified as it is the BLR, but emission lines coming from the same region (like the doublets and the Balmer lines) should display similar widths. For this reason, velocity widths for narrow lines were tied together to the same value for each doublet as well as for the narrow components (and broad, if any) of the Balmer lines. The results from the spectral fitting of the two objects are shown in Table 2 and the optical fitted spectra are shown in Figs 1 and 2.

In the case of Q2130−431, a broad component with an FWHM $\sim$ 9700 km s^{-1} is clearly detected in the Hα and Hβ emission lines. According to the Whittle (1992) classification criteria for intermediate-type Seyfert galaxies [based on the $F_{\rm [O III]}/F_{\rm H\beta(broad)}$ ratio], Q2130−431 should be classified as Seyfert 1.5. However, $F_{\rm [O III]}/F_{\rm H\beta(broad)} = 1.0$ is close to the boundary between the Seyfert 1.5 and Seyfert 1.8 classification; since the Seyfert 1.5 classification is mainly used for sources with highly variable spectra, we adopt a Seyfert 1.8 classification for Q2130−431.

Conversely, no broad components (Hα nor Hβ) are significantly detected in the spectra of Q2131−427. We compute an upper limit on the Hα and Hβ broad emission line components by fixing the linewidths to 4000 km s^{-1}, a conservative value for BLR widths (Ho et al. 1997). We are confident that in this source the lack of detection of broad line components is not due to the host galaxy contamination. Indeed, our spectra are quite flat and do not show any significant contribution from the host galaxy. Since the data are taken in long-slit mode, we are able to extract only the most central part of the source, thus avoiding as much as possible the host galaxy contribution.

We calculate the fractional contribution of the Hα broad component to the total (broad+narrow) Hα emission by using the estimated upper limit. This corresponds to at the most 30 per cent, a low value if compared to the average value in the Ho et al. (1997) Seyfert sample which is around 65 per cent. Note that the latter is a conservative estimate since the average FWHM for broad line components in Ho et al. (1997) is around 2700 km s^{-1} while our upper limit has been calculated for a FWHM of 4000 km s^{-1}.
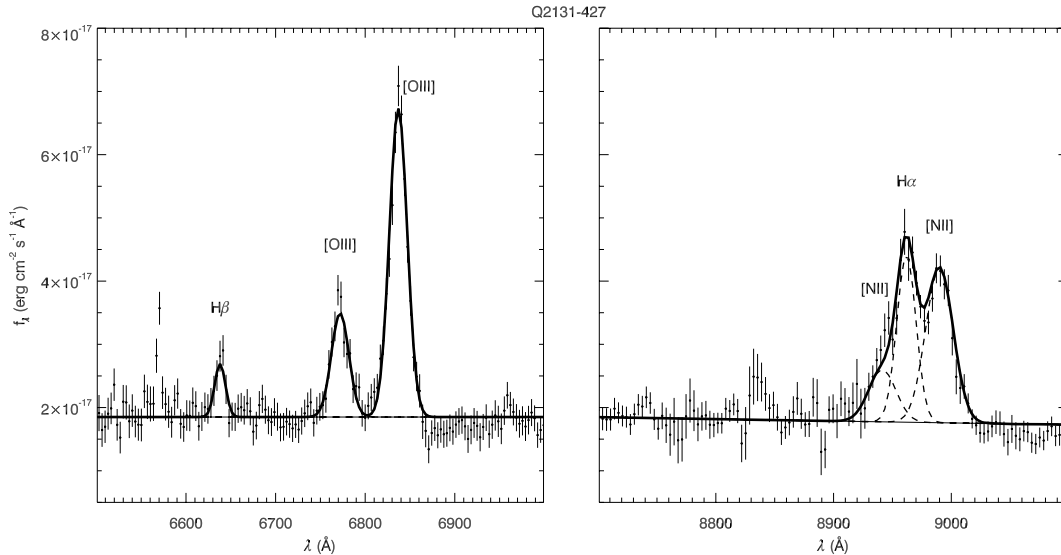
Figure 2. Q2131−427 EMMI optical spectrum. Best-fitting models of the Hβ (left-hand panel) and Hα (right-hand panel) spectral regions.

In the classical [O III]/Hβ versus [N II]/Hα diagnostic diagram plot used to classify narrow emission line galaxies (Kewley et al. 2006), both sources are placed in the Seyfert region, well above the low-ionization nuclear emission region–starburst limits. In conclusion, the optical classification for Q2130−431 and Q2131−427 is Seyfert 1.8 and Seyfert 2, respectively.

It is interesting to compare our spectral results with those obtained from Hawkins (2004) and here reported within parenthesis in Table 2. The [O III] and Hβ FHWM measured for Q2130−431 are consistent with the ones reported in Hawkins (2004), after spectral resolution correction, while our measured [O III]/Hβ ratio of ∼11 is smaller compared to ∼16 (see Table 1). In the optical spectrum of Q2131−427, the major difference results in the Hβ FWHM significantly smaller than the one measured by Hawkins (2004) (∼830 km s^{-1}). On the other hand, the [O III]/Hβ ratio of ∼9 and the [O III] width are consistent within errors. We note that this comparison exercise should be taken with caution, since the quality of the spectroscopy observations in Hawkins (2004), performed with 2dF multifibre spectrograph, cannot provide accurate error estimates for the FWHM and could also be problematic when calculating line ratios, given the unreliability of sky subtraction and flux calibration.

3.2 *XMM–Newton* observations

Q2130−431 and Q2131−427 were observed by *XMM–Newton* on 2006 November (Obs ID: 0402460201). Data have been processed starting from the observation data fits files with SAS 7.0.0. X-ray events corresponding to patterns 0–12 and 0–4 were selected from the EPIC-MOS and EPIC-pn cameras, respectively. We used the most updated calibration files available at the time of the reduction for each source data. Source light curves and spectra were extracted from circular regions of 25 arcsec centred on the source, while background products were obtained from off-set regions close to the source. Exposure times have been filtered out for periods of high background, and the 'good time interval' exposures are reported in Table 1 as well as the observation date and the instruments filters. Spectra were binned according to the counts collected in each source. The ancillary and detector response matrices were generated using the *XMM–Newton* SAS ARFGEN and RMFGEN tasks. The X-ray

light curves have been examined and no significant variability has been found.

The pn, MOS1 and MOS2 spectra were analysed using XSPEC v.12.4.0. Galactic absorption is implicitly included in all spectral models. Abundances are those of Anders & Grevesse (1989). The errors, lower and upper limits quoted correspond to 90 per cent confidence range for one interesting parameter (i.e. $\Delta\chi^2 = 2.71$; Avni 1976), unless otherwise stated.

The X-ray spectrum of Q2130−431 is well represented by a single power law with photon spectral index $\Gamma = 1.77 \pm 0.04$ ($\chi^2/\nu = 150/144$). No extra absorption apart from the Galactic one is needed ($N_{H,int} < 2 \times 10^{20}$ cm^{-2}). Q2131−427 shows a very weak spectrum, modelled by a single power law ($\Gamma \sim 2$) and an upper limit (at 90 per cent confidence level) on the intrinsic absorption of $N_{H,int} < 9 \times 10^{20}$ cm^{-2}. We fixed a narrow Gaussian emission line at the rest energy of the FeKα line, 6.4 keV, and we measured an upper limit on the equivalent width of the line of ∼2 keV. However, this large value is probably due to the significant residuals visible above 5 keV in the pn spectrum; actually, the very low photon statistics around 6–7 keV and the background dominance in this range prevent us from drawing any strong conclusions based on this limit. In Figs 3 and 4, best-fitting spectra are shown on the left-hand panels, while column density versus photon index contour plots are on the right-hand panels. In Table 3, we show the best-fitting parameters together with the model fluxes and luminosities in the 0.5–2 keV and 2–10 keV bands. We also report the black hole mass derived from the M_{BH}–$\sigma_\star$ relation (Tremaine et al. 2002), where $\sigma_\star$ is the stellar velocity dispersion obtained from the FWHM([O III]) as shown in Greene & Ho (2005). The Eddington ratio has been calculated assuming that $L_{Bol}/L_X = 20$ (Elvis et al. 1994; Vasudevan & Fabian 2009).

4 DISCUSSION

The 'naked' AGN as discovered by Hawkins (2004) are among the best candidates to look for 'true' unabsorbed Seyfert 2 galaxies (Panessa & Bassani 2002). Indeed, the monitored optical variability over 25 yr points to a nucleus seen directly where, given the absence of broad optical emission lines in the optical spectra, the BLR may lack. As successfully proven for NGC 3147 (Bianchi et al. 2008),
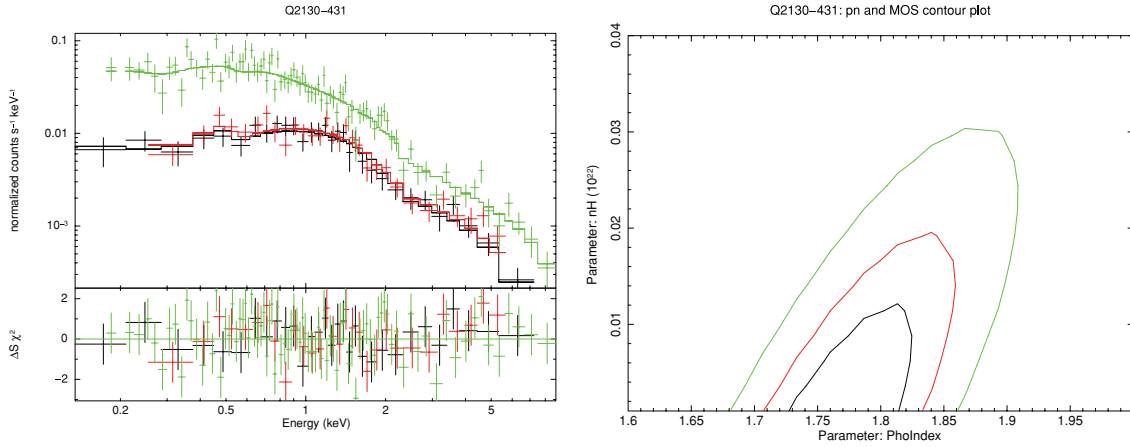
Figure 3. *XMM–Newton* observation of Q2130−431. Left-hand panel: the EPIC pn, MOS1 and MOS2 spectra, best-fitting models and $\Delta\chi^2$ deviations. Right-hand panel: column density versus photon index contour plots at 68, 90 and 99 per cent confidence level for two interesting parameters.
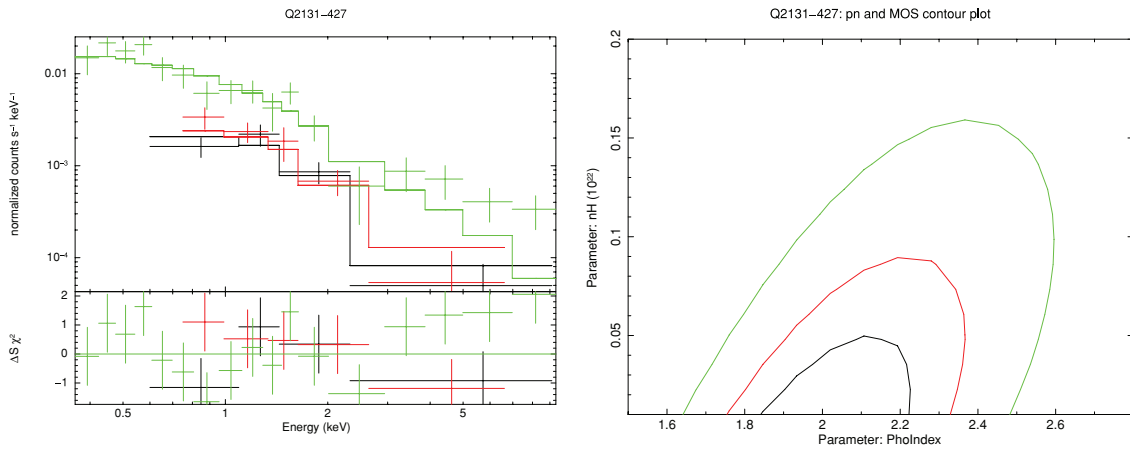

Figure 4. *XMM–Newton* observation of Q2131−427. Left-hand panel: the EPIC pn, MOS1 and MOS2 spectra, best-fitting models and $\Delta\chi^2$ deviations. Right-hand panel: column density versus photon index contour plots at 68, 90 and 99 per cent confidence level for two interesting parameters.

Table 3. *XMM–Newton* spectral parameters, black hole mass and Eddington ratio.

Name	$N_{\rm H,Gal}$	$N_{\rm H,int}$	Γ	χ^2/d.o.f.	$F_{0.5-2}$ (cgs)	F_{2-10} (cgs)	$L_{0.5-2}$ (cgs)	L_{2-10} (cgs)	$M_{\rm BH}$ $\rm M_\odot$	$L_{\rm Bol}/L_{\rm Edd}$
(1)	(2)	(3)	(4)	(5)	(6)	(7)	(8)	(9)	(10)	(11)
Q2130−431	2.4	<2.0	$1.77^{+0.04}_{-0.04}$	149.8/144	7.9×10^{-14}	1.5×10^{-13}	2.0×10^{43}	3.8×10^{43}	1.6×10^7	0.37
Q2131−427	2.2	<9.0	$2.00^{+0.23}_{-0.21}$	27.3/23	1.8×10^{-14}	2.2×10^{-14}	1.0×10^{43}	1.2×10^{43}	7.7×10^8	2.4×10^{-3}

Notes. Column (1): name of the source; Column (2): Galactic column density in units of 10^{20} (cm^{-2}); Column (3): intrinsic column density in units of 10^{20} (cm^{-2}); Column (4): photon index; Column (5): chi-squared and degrees of freedom; Column (6): intrinsic flux in the 0.5–2 keV band; Column (7): intrinsic flux in the 2–10 keV band; Column (8): intrinsic luminosity in the 0.5–2 keV band; Column (9): intrinsic luminosity in the 2–10 keV band; Column (10): black hole mass; Column (11): ratio of bolometric to Eddington luminosity.

the key strategy to spot this class of AGN is through simultaneous optical and X-ray observations in order to rule out variability as the cause of the optical and X-ray mismatch. We have therefore observed two 'naked' AGN candidates, Q2130−431 and Q2131−427, simultaneously in the X-ray and optical band.

4.1 Q2131−427: a 'true' unabsorbed Seyfert 2 galaxy

For Q2131−427, the photometric measurements obtained over ∼25 yr, as reported in Hawkins (2004), show a slow decrease of the

emission, from $B \sim 20$ mag in 1974 to $B \sim 21$ mag in 2002. The Optical Monitor on board *XMM–Newton* (Mason et al. 2001) measured $B = 20.83 \pm 0.10$, only slightly above the last measurement in the $B_{\rm J}$ light curve (in 2001) $B_{\rm J} = 21.2 \pm 0.3$, confirming that the source is still in a low flux state. Interestingly, Q2131−427 shows no signs of broad emission line components in its optical spectrum and the faint X-ray spectrum of this source is unabsorbed, with an upper limit on the intrinsic column density of $N_{\rm H,int} < 9 \times 10^{20}$ cm^{-2}, consistent with that from a host galaxy. This picture is hard to reconcile within the Unified Model predictions, where the BLR

is obscured by a toroidal absorbing medium of dust and gas, the former responsible of the optical extinction of the broad emission lines and the latter measurable in X-rays.

One possibility is that the BLR is hidden behind a Compton-thick medium whose column density cannot be measured in X-ray spectra below 10 keV (Matt, Pompilio & La Franca 1999). The upper limit on the EW of the FeKα line at 6.4 keV does not rule out the Compton-thick hypothesis, however this measurement is not reliable, given the low statistics spectrum above 5 keV. Instead, the $F_{2-10\text{keV}}/F_{[\text{O\,III}]}$ ratio[2] of $\sim$6 is typical of Compton-thin sources.

Tran (2001) studied the properties of type 2 Seyfert galaxies with polarized (hidden) BLRs (HBLRs) seen in reflected light compared to the non-HBLR Seyfert 2 galaxies, introducing the use of a diagnostic diagram involving [O\,III]λ5007/Hβ. The median values of [O\,III]λ5007/Hβ found are 6.8 ± 1.5 and 9.9 ± 1.3 for the non-HBLR and HBLR Seyfert 2 galaxies, respectively. The [O\,III]λ5007/Hβ ratio of Q2131$-$427 is $\sim$9, suggesting that this source might harbour a hidden BLR. In this hypothesis, some sort of dusty medium should obscure the optical broad emission lines and be gas-free.

As already invoked for the unabsorbed Seyfert 2 in Panessa & Bassani (2002), a dust-to-gas ratio of 10–50 times higher than Galactic would be enough to obscure the BLR. However, this is an unlikely scenario as a dust obscuration is often observed to be lower than the associated gas column density (see Maiolino et al. 2001). Moreover, the Balmer decrement of the NLR, i.e. (Hα/Hβ)$_\text{NLR} \sim$ 4.2, suggests that the environment is not particularly dusty (Ward et al. 1987) and the optical extinction $A_V \sim 1.3$ mag derived from the Balmer decrement is still too small to be able to completely obscure a standard BLR.

The hypothesis of a pc and/or sub-pc scale clumpy obscuring medium which results in a variable column density in X-ray spectra (Risaliti, Elvis & Nicastro 2002; Elvis et al. 2004; Risaliti et al. 2005; Bianchi et al. 2009) cannot help to explain the complete absence of broad components in the optical spectrum. On the assumption that the X-ray absorption originates from the BLR clouds (see Risaliti et al. 2009), we should expect variable column density in the X-ray spectra but still broad emission lines in the optical spectrum, indeed at these spatial scales the gas should be dust-free being within the sublimation radius.

The most likely explanation for the observed optical/X-ray discrepancy is to assume that in this source the BLR does not exist or its emission is gradually declining. Indeed, the well-documented optical flux decrease may favour the hypothesis that the BLR fades away in response to a decrease of the continuum emission. Recent models propose a dependence of the BLR properties with luminosity and/or accretion rate (Williams et al. 1999; Nicastro 2000; Nicastro et al. 2003; Elitzur & Shlosman 2006; Wang & Zhang 2007). According to Elitzur & Shlosman (2006), the classical molecular torus is just the outer part of a clumpy wind that comes out off the accretion disc. At bolometric luminosities lower than $\sim$10^{42} erg s^{-1}, the mass accretion can no longer sustain the cloud outflow rate causing the disappearance of the torus and, at lower luminosities, of the broad line clouds too. According to the above scheme, the absence of a BLR in Q2131$-$427 is not justified given the high bolometric luminosity ($L_\text{Bol} \sim 8 \times 10^{44}$ erg s^{-1}); however, the low Eddington ratio measured ($L_\text{Bol}/L_\text{Edd} = 0.0024$) may favour the scenario in which the BLR is formed in a vertical disc wind originating at a critical distance in the accretion disc, at accretion rates higher than

a minimum value ($\sim$10^{-3}; Nicastro 2000). According to this model, below the critical accretion rate the BLR cannot be formed. In the case of Q2131$-$427, this is one of the best hypotheses to interpret the observational mismatch, taking into account that the Eddington ratio is around this critical value and it is probably affected by uncertainties related to the determination of the black hole mass and of the bolometric correction. If the BLR properties actually depend on the luminosity and/or accretion physics, this must have strong implications for AGN Unification Models and also for population studies of obscured and unobscured AGN samples (e.g. fraction of type 2 objects versus luminosity) as discussed in Elitzur & Shlosman (2006) [see also Wang & Zhang (2007) for an evolutionary sequence of Seyfert galaxies].

4.2 Q2130$-$431: a 'true' intermediate Seyfert galaxy?

The Q2130$-$431 optical spectrum shown here reveals that this source is a type 1.8 Seyfert galaxy, i.e. we detect Hα and Hβ broad line components (see Fig. 1). The Hα broad component was not detected by Hawkins (2004) since, at the redshift of the source, the line is shifted out of their optical spectra. Also the Hβ broad component was not detected, maybe because it was difficult to identify given its broadness, being hidden under a galaxy continuum (see fig. 6 in Hawkins 2004). Alternatively, it may be variable. Note that the FWHM of the Hβ narrow line component has not varied significantly between 2002 ($\sim$426 km s^{-1}) and 2006 (320^{+50}_{-30} km s^{-1}) observations.

The simultaneous ultraviolet imaging with the Optical Monitor allows us to detect the source in the UVW1 filter (245–320 nm), with a Galactic reddening corrected magnitude of 20.11 $\pm$ 0.07, slightly brighter when compared to the last measurement of $B_\text{J} = 20.35 \pm 0.05$ mag, as shown in the 25 yr light curve (see fig. 8, Hawkins 2004). In X-rays, the 2–10 keV luminosity of $\sim$4 $\times$ 10^{43} erg s^{-1} suggests that this is a typical type 1 Seyfert galaxy with a standard photon index ($\Gamma = 1.8$–2; e.g. Piconcelli et al. 2005) and no intrinsic absorption ($< 2 \times 10^{20}$ cm^{-2}, at 90 per cent confidence level). The $F_{2-10\text{keV}}/F_{[\text{O\,III}]}$ ratio is $\sim$77, well within the regime of Compton-thin objects (Bassani et al. 1999; Cappi et al. 2006). Our X-ray flux is in agreement with the *Chandra* one found by Gliozzi et al. (2007) suggesting no particular variability in X-rays.

According to the above observational evidence, Q2130$-$431 should not be considered as a pure 'naked' AGN, in the sense that it displays optical broad emission line components and, therefore, it has a BLR. However, intermediate type Seyfert galaxies are characterized by large Balmer decrements consistent with reddening of the BLR and determining the 1.8/1.9 spectroscopic type (Osterbrock 1981). The weakness of the broad Balmer lines is often ascribed to dust absorption (Maiolino & Rieke 1995) and, indeed, moderate absorption is observed in X-rays (Risaliti et al. 1999). In Q2130$-$431, the optical BLR Balmer decrement of 3.4 (almost the same value of the NLR Balmer decrement) suggests that the BLR does not suffer from heavy reddening. In addition, in the X-ray spectrum, no absorption has been measured, strengthening the idea that the BLR is not obscured and that the weakness of the broad optical lines can be intrinsic, e.g. due to a small amount of gas in the clouds. A weak BLR can be due to a luminosity/accretion rate related disappearance, as suggested for Q2131$-$427. Interestingly, the existence of this kind of objects should be hypothesized within an evolutionary sequence, as the one drawn in Elitzur & Shlosman (2006), from type 1 objects to 'true' type 2s. However, the high X-ray luminosity and the Eddington ratio ($L_\text{Bol}/L_\text{Edd} \sim 0.37$) disfavour the latter hypothesis. Alternatively, the lack of a prominent

---

[2] $F_{[\text{O\,III}]}$ has been reddening corrected (Bassani et al. 1999).

BLR in Q2130−431 may simply be a peculiar intrinsic property of this object. In both scenarios, Q2130−431 can represent a case of 'true' intermediate Seyfert galaxy, in which the BLR is intrinsically weak instead of being obscured by dust or gas.

5 CONCLUSIONS

We have obtained quasi-simultaneous X-ray (*XMM–Newton*) and optical (NTT–EMMI) spectra of two Seyfert galaxies, Q2130−431 and Q2131−427, belonging to the class of 'naked' AGN characterized by Hawkins (2004) and, currently, composed of six members. The strong optical brightness variability and the lack of broad emission line components in their spectra have suggested that in these AGN the nucleus is seen directly and it is taken off its BLR. Our quasi-simultaneous observations have proven fundamental to confirm the 'naked' hypothesis in the case of Q2131−427, for which we have ruled out the Compton-thick nature based on the low $F_{2-10\,\mathrm{keV}}/F_{[\mathrm{O\,III}]}$ ratio. Moreover, the Balmer decrement in the NLR excludes a high dust-to-gas ratio as a possible explanation of the broad emission lines absence. Instead, the present observations have confirmed that no broad components are found associated with the optical spectrum emission lines and simultaneously no absorption is measured in the X-ray spectrum. Either a dusty medium is absorbing the BLR being adequately gas-free to let the X-ray continuum escape, however this is an unlikely scenario, or the source is accreting below a critical accretion rate such that the BLR cannot be formed (Nicastro 2000).

The 'naked' hypothesis is instead discarded for Q2130−431, which indeed displays Hα and Hβ broad line components in its optical spectrum. However, no sign of mild absorption in its X-ray continuum is found, contrary to what expected for intermediate Seyfert galaxies (in order to justify the partial obscuration of the BLR), neither the BLR itself seems to suffer from heavy reddening. The presence of a small amount of gas to photoionize can be the reason for the intermediate optical spectrum, making it a case of a potential 'true' intermediate Seyfert galaxy.

Finally, in the Appendix, we present the results on the cluster Abell 3783 serendipitously detected in the Q2131−427 EPIC FOV providing a description of its fundamental parameters.

REFERENCES

Allen S. W., Fabian A. C., 1998, A&A, 297, L57
Anders E., Grevesse N., 1989, Geochim. Cosmochim. Acta, 53, 197
Antonucci R., 1993, ARA&A, 31, 473
Avni Y., 1976, ApJ, 210, 642

Awaki H., Koyama K., Inoue H., Halpern J. P., 1991, PASJ, 43, 195
Barcons X., Carrera F. J., Ceballos M. T., 2003, MNRAS, 339, 757
Bartelmann M., Steinmetz M., 1996, MNRAS, 283, 431
Bassani L., Dadina M., Maiolino R., Salvati M., Risaliti G., della Ceca R., Matt G., Zamorani G., 1999, ApJS, 121, 473
Bianchi S., Corral A., Panessa F., Barcons X., Matt G., Bassani L., Carrera F. J., Jiménez-Bailón E., 2008, MNRAS, 385, 195
Bianchi S., Piconcelli E., Chiaberge M., Bailón E. J., Matt G., Fiore F., 2009, ApJ, 695, 781
Brightman M., Nandra K., 2008, MNRAS, 390, 1241
Bryan G. L., Norman M. L., 1998, ApJ, 495, 80
Caccianiga A. et al., 2004, A&A, 416, 901
Cappi M. et al., 2006, A&A, 446, 459
Cavaliere A., Fusco-Femiano R., 1976, A&A, 49, 137
Corral A., Barcons X., Carrera F. J., Ceballos M. T., Mateos S., 2005, A&A, 431, 97
De Grandi S., Molendi S., 2001, ApJ, 551, 153
Dickey J. M., Lockman F. J., 1990, ARA&A, 28, 215
Elitzur M., Shlosman I., 2006, ApJ, 648, L101
Elvis M. et al., 1994, ApJS, 95, 1
Elvis M., Risaliti G., Nicastro F., Miller J. M., Fiore F., Puccetti S., 2004, ApJ, 615, L25
Ettori S., 2000, MNRAS, 311, 313
Ettori S., Balestra I., 2009, A&A, 496, 343
Fiore F. et al., 2001, MNRAS, 327, 771
Gastaldello F., Buote D. A., Humphrey P. J., Zappacosta L., Bullock J. S., Brighenti F., Mathews W. G., 2007, ApJ, 669, 158
Gastaldello F., Trevese D., Vagnetti F., Fusco-Femiano R., 2008, ApJ, 673, 176
Gliozzi M., Sambruna R. M., Foschini L., 2007, ApJ, 662, 878
Greene J. E., Ho L. C., 2005, ApJ, 627, 721
Guainazzi M., 2008, XMM-SOC-CAL-TN-0018 issue 2.7
Guainazzi M., Fabian A. C., Iwasawa K., Matt G., Fiore F., 2005, MNRAS, 356, 295
Hawkins M. R. S., 2004, A&A, 424, 519
Ho L. C., Filippenko A. V., Sargent W. L. W., Peng C. Y., 1997, ApJS, 112, 391
Kewley L. J., Groves B., Kauffmann G., Heckman T., 2006, MNRAS, 372, 961
Kuntz K. D., Snowden S. L., 2008, A&A, 478, 575
Lin Y.-T., Mohr J. J., 2004, ApJ, 617, 879
Maiolino R., Rieke G. H., 1995, ApJ, 454, 95
Maiolino R., Marconi A., Salvati M., Risaliti G., Severgnini P., Oliva E., La Franca F., Vanzi L., 2001, A&A, 365, 28
Markevitch M., 1998, ApJ, 504, 27
Mason K. O. et al., 2001, A&A, 365, L36
Mateos S., Barcons X., Carrera F. J., Ceballos M. T., Hasinger G., Lehmann I., Fabian A. C., Streblyanska A., 2005, A&A, 444, 79
Mateos S. et al., 2009, A&A, 496, 789
Matt G., Pompilio F., La Franca F., 1999, New Astron., 4, 191
Matt G., Guainazzi M., Maiolino R., 2003, MNRAS, 342, 422
Nicastro F., 2000, ApJ, 530, L65
Nicastro F., Martocchia A., Matt G., 2003, ApJ, 589, L13
Oke J. B., 1990, AJ, 99, 1621
Osterbrock D. E., 1981, ApJ, 249, 462
Panessa F., Bassani L., 2002, A&A, 394, 435
Pappa A., Georgantopoulos I., Stewart G. C., Zezas A. L., 2001, MNRAS, 326, 995
Piconcelli E., Jimenez-Bailón E., Guainazzi M., Schartel N., Rodríguez-Pascual P. M., Santos-Lleó M., 2005, A&A, 432, 15
Risaliti G., Maiolino R., Salvati M., 1999, ApJ, 522, 157
Risaliti G., Elvis M., Nicastro F., 2002, ApJ, 571, 234
Risaliti G., Elvis M., Fabbiano G., Baldi A., Zezas A., 2005, ApJ, 623, L93
Risaliti G., Elvis M., Fabbiano G., Baldi A., Zezas A., Salvati M., 2007, ApJ, 659, L111
Risaliti G. et al., 2009, MNRAS, 393, L1
Roncarelli M., Ettori S., Dolag K., Moscardini L., Borgani S., Murante G., 2006, MNRAS, 373, 1339

Shuder J. M., Osterbrock D. E., 1981, ApJ, 250, 55
Spergel D. N. et al., 2003, ApJS, 148, 175
Tran H. D., 2001, ApJ, 554, L19
Tremaine S. et al., 2002, ApJ, 574, 740
Vasudevan R. V., Fabian A. C., 2009, MNRAS, 392, 1124
Vikhlinin A. et al., 1999, ApJ, 525, 47
Vikhlinin A. et al., 2006, ApJ, 640, 691
Voges W. et al., 1999, A&A, 349, 389
Wang J.-M., Zhang E.-P., 2007, ApJ, 660, 1072
Ward M., Elvis M., Fabbiano G., Carleton N. P., Willner S. P., Lawrence A., 1987, ApJ, 315, 74
West R. M., Fradsen S., 1981, A&AS, 44, 329
Whittle M., 1992, ApJS, 79, 49
Williams R. J. R., Baker A. C., Perry J. J., 1999, MNRAS, 310, 913
Wolter A., Gioia I. M., Henry J. P., Mullis C. R., 2005, A&A, 444, 165

APPENDIX A: THE SERENDIPITOUS DETECTION OF X-RAY EMISSION BY THE CLUSTER ABELL 3783

An extended source, of a $\sim$3-arcmin scale, in the field of Q2131−427 is clearly detected at 10.2-arcmin off-axis (see Fig. A1). The X-ray peak of the source in equatorial coordinates is $\alpha_{J2000.0} = 21^{\rm h}34^{\rm m}00^{\rm s}.7$, $\delta_{J2000.0} = -42°38'46''$ and it is associated with the cluster of galaxies Abell 3783 (see the overlay of the X-ray contours on the Digitized Sky Survey (DSS) image in Fig. A1) at the redshift of $z = 0.195$ (West & Fradsen 1981). With the caveat of the *XMM–Newton* point spread function (PSF) at this off-axis angle ($\sim$8 arcsec is the 50 per cent encircled energy fraction radius at 1.5 keV), the peak is consistent with being associated with the brightest cluster galaxy (BCG), 2MASX J21335944−4238448, rather than the likely interloper 2MASX J21340071−4238528 with position $\alpha_{J2000.0} = 21^{\rm h}34^{\rm m}00^{\rm s}.7$, $\delta_{J2000.0} = -42°38'53''$ at a redshift $z = 0.028$. These are the only galaxies with redshifts available listed in NED within 3 arcmin of the source. Considerations of the redshift derived from the Fe Kα complex in the X-ray spectrum, the luminosity and the temperature of the cluster give further strength to the association. In the following, we will therefore assume $z = 0.195$ as the redshift of the source for which 1 arcmin corresponds to 194 kpc. All the errors quoted in this Appendix are at the 68 per cent confidence limit.

The data reduction and preparation follow the procedure of Gastaldello et al. (2008) where more details can be found; here we provide just a brief description. The data were re-processed with SAS v8.0.

For each detector, we created images in the 0.5–2 keV band with point sources masked using circular regions of 25-arcsec radius centred at the source position. The images have been exposure corrected and a radial surface brightness profile was extracted from a circular region of 7 arcmin of radius centred on the cluster centroid. We account for the X-ray background in the surface brightness analysis by including a constant-background component. The data were grouped to have at least 20 counts per bin in order to apply the χ^2 statistic. The fitted model is convolved with the *XMM–Newton* PSF. The joint best-fitting β model (Cavaliere & Fusco-Femiano 1976) has a core radius of $r_{\rm c} = 120 \pm 13$ kpc (37$\pm$4 arcsec) and $\beta = 0.54 \pm 0.03$ for a χ^2/d.o.f. = 210/141 (see Fig. A2). Fits to the profiles of the individual detectors give consistent results within 1σ of the combined-fit result and in the case of the MOS2 detector is formally acceptable (49/47). The main contribution to the χ^2 comes mainly from the pn (χ^2/d.o.f. = 102/61 for the fit to the individual profile) and its origin is instrumental (CCD gaps and pixels undersampling the PSF), whereas a large area of the radial profile at $r >$ 5 arcmin is lost for MOS1 (χ^2/d.o.f. = 55/29) due to the missing CCD-6, hence there is no need for more complicated models.

For spectral fitting, we extracted spectra for each detector from a 2.5-arcmin region centred on the peak of the emission, to maximize the signal-to-noise ratio (S/N) over the background. Redistribution matrix files and ancillary response files were generated using the SAS tasks RMFGEN and ARFGEN in extended source mode with appropriate flux weighting. The background was estimated locally using spectra
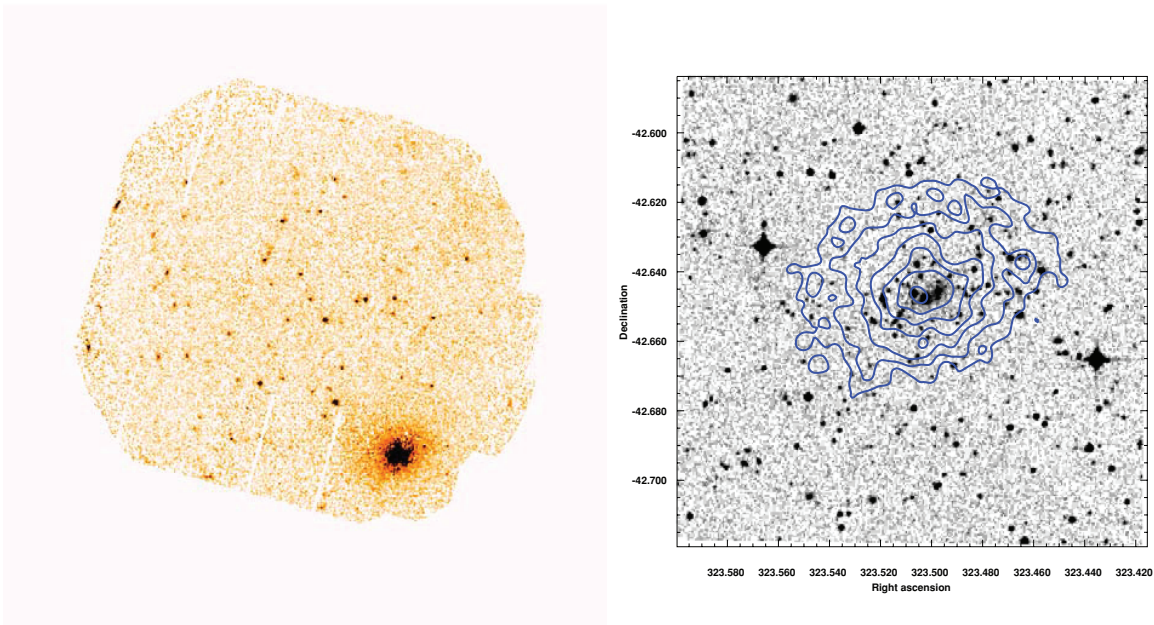

Figure A1. Left: exposure corrected 0.5–2.0 keV combined MOS1, MOS 2 and pn X-ray image of the field of Q2131−427. The cluster is clearly visible as the extended source near the edge of the field of view. Right: the DSS image of the cluster with X-ray contours overlaid and logarithmically spaced between 5×10^{-6} and 5×10^{-5} counts s^{-1} pixel^{-1}. Equatorial coordinates are given at J2000 equinox.
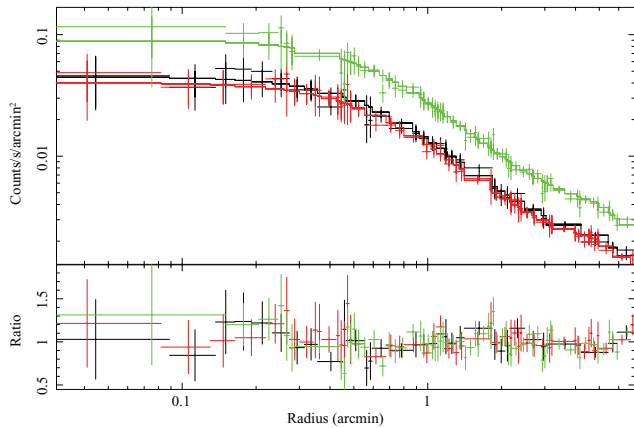
Figure A2. Surface brightness profile of the X-ray emission of Abell 3783. Data from MOS1, MOS2 and pn are plotted in black, red and green, respectively. The best-fitting β model and ratio of data over the model are also shown.
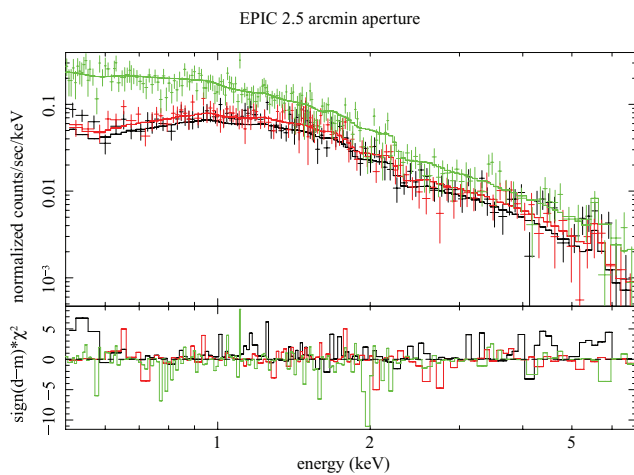

Figure A3. X-ray spectrum of the Abell 3783 taken from a 2.5-arcmin aperture centred on the peak of the emission. Data from MOS1, MOS2 and pn are plotted in black, red and green, respectively. The best-fitting model and residuals are also shown.

extracted from a source-free region of the same extent at the same off-axis angle (avoiding CCD-4 for MOS1 and CCD-5 for MOS 2 because in this observation they display anomalous background for energies below 1 keV; see Kuntz & Snowden 2008). The spectra from the three detectors were re-binned to ensure a S/N of at least 3 and a minimum 20 counts per bin and they were jointly fitted with an APEC thermal plasma modified by Galactic absorption (Dickey & Lockman 1990). The spectral fitting was performed in the 0.5–7 keV band. The spectra are shown in Fig. A3: the best-fitting parameters are $kT = 4.94 \pm 0.25$ keV and $Z = 0.32 \pm 0.02\,Z_\odot$ for a χ^2/d.o.f. = 418/396. The source photons correspond to about 78 per cent of the total events ($\sim$3400 counts in each MOS and 5700 in the pn). If we leave the redshift parameter free, we obtain $z = 0.20 \pm 0.01$, in good agreement with the redshift determined optically: the quality of the *XMM–Newton* data is such to tightly constrain the redshift of the cluster; in Fig. A4, we show the temperature–redshift and redshift–metal abundance χ^2 confidence contours.

A likely previous X-ray identification is the *ROSAT* source 1RXS J213401−423833 in the *ROSAT* All-Sky bright source catalogue (Voges et al. 1999) and associated with Abell 3783. The *ROSAT*

count rate of $6.32 \pm 1.61 \times 10^{-2}$ counts s^{-1}, which corresponds to an unabsorbed flux in the 0.1–2.4 keV band of $1.04 \pm 0.30 \times 10^{-12}$ erg cm^{-2} s^{-1} (for a 5-arcmin extraction radius), is in good agreement with our determination of $1.30 \pm 0.05 \times 10^{-12}$ in the 0.1–2.4 keV band (according to the derived surface brightness model, the 2.5–5 arcmin region contributes only $\sim$25 per cent of the flux within a 5-arcmin region).

To investigate possible spatial variation in the spectral parameters of the cluster, we extracted two annular regions of radii 0–1 and 1–3 arcmin. The derived spectral parameters are: $kT = 4.78 \pm 0.28$ keV and $Z = 0.51 \pm 0.13\,Z_\odot$ with χ^2/d.o.f. = 226/177 for the inner annulus; $kT = 4.50^{+0.40}_{-0.35}$ keV and $Z = 0.09^{+0.11}_{-0.09}\,Z_\odot$ with χ^2/d.o.f. = 313/314 for the outer annulus. The width of the bins have been chosen in order to avoid bias in the temperature measurement caused by scattered flux by the PSF. It is difficult, given the off-axis position of the cluster, to assess the existence of gradients in the temperature: given the quality of the data, the cluster is consistent with being isothermal over the explored radial range. The abundance gradient, signature of relaxed cool-core cluster (e.g. De Grandi & Molendi 2001), is on the contrary significant at the 2.6σ level.

Under the assumption of isothermality and assuming that the cluster follows the best-fitting model to the surface brightness profile derived above, we can calculate the total mass profile using the best-fitting β model for which the gas density and total mass profiles can be expressed by simple analytical formula (e.g. Ettori 2000). We evaluated r_{500} as the radius at which the density is 500 times the critical density and the virial radius as the radius at which the density corresponds to Δ_{vir}, as obtained by Bryan & Norman (1998)[3] for the concordance cosmological model used in this paper. To evaluate the errors on the estimated quantities, we used the same procedure as above repeating the measurements for 10 000 random selections drawn from Gaussian distributions for the temperature and parameters of the surface brightness profile. For $\Delta = 500$, we obtained $M_{500} = (2.69 \pm 0.31) \times 10^{14}\,\text{M}_\odot$ within $r_{500} = 920 \pm 36$ kpc; the virial mass $M_{\text{vir}} = (5.65 \pm 0.65) \times 10^{14}\,\text{M}_\odot$, within the virial radius $r_{\text{vir}} = 1911 \pm 73$ kpc. If the identification of 2MASX J21335944−4238448 with the BCG is correct, the optical luminosity calculated in the K_{S} following Lin & Mohr (2004) is $M_{K_{\text{S}}} = -27.02$ corresponding to $1.40 \times 10^{12}\,\text{L}_\odot$, consistent with the central galaxy luminosity–host halo mass relation (and its scatter) derived in the literature (e.g. Lin & Mohr 2004). We calculated the gas mass to be $M_{\text{gas},500} = (3.37 \pm 0.37) \times 10^{13}\,\text{M}_\odot$. For Abell 3783, the aperture of 485 kpc used for spectroscopy encloses 74 per cent of the flux within r_{500}. The derived bolometric luminosity within r_{500} is $L_{500} = (3.61 \pm 0.26) \times 10^{44}$ erg s^{-1}: Abell 3783 lies very close to the L_{X}–T_{X} relation derived from the cluster sample of objects with $T_{\text{X}} > 3$ keV of Markevitch (1998), though given the angular resolution of the data it has not been possible to correct for the effect of an eventual presence of a cool core (Allen & Fabian 1998; Markevitch 1998).

Finally, as done routinely in our previous analysis (e.g. Gastaldello et al. 2007, 2008), we have studied the sensitivity of our results to various systematic uncertainties and data analysis choices that may impact our results, like varying N_{H} or using a different energy band (1–7 keV) or standard blank background fields for background subtraction, finding always agreement within the errors with the results reported above. Below, we summarize two possible sources of errors not previously explored in our work.

---

[3] $\Delta_{\text{vir}} = 18\pi^2 + 82x - 39x^2$, where $x = \Omega(z) - 1$, $\Omega(z) = \Omega_{\text{m}}(1 + z)^3/E(z)^2$ and $E(z) = [\Omega_{\text{m}}(1 + z)^3 + \Lambda]^{1/2}$
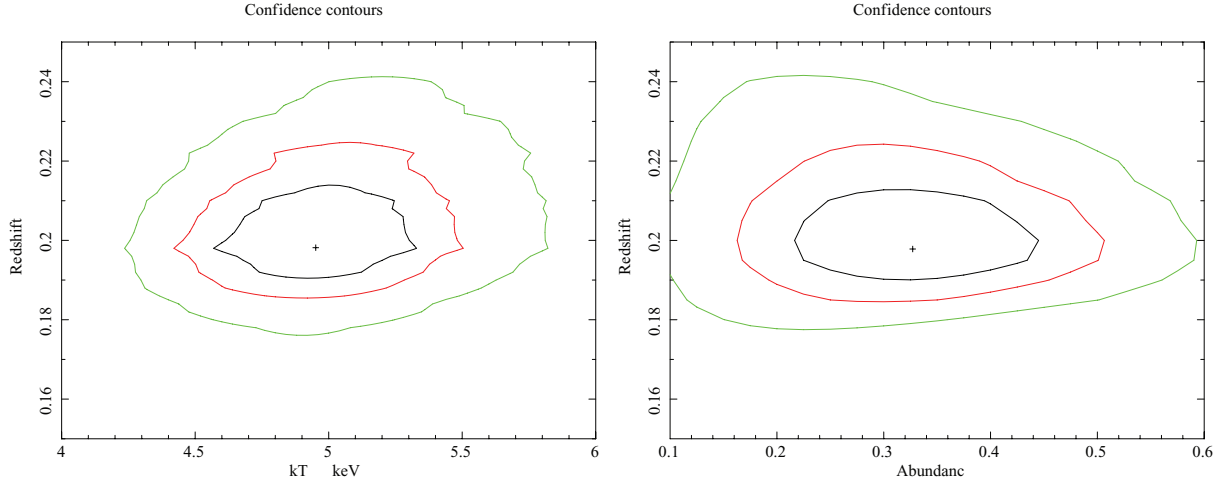
Figure A4. The 68, 90 and 99 per cent redshift–temperature χ^2 contours on the left-hand panel and redshift abundance on the right-hand panel derived from the spectrum of Fig. A3.

Cross-calibration. Improvements have been made in the status of the cross-calibration between the EPIC cameras in the recent SAS releases, but some calibration differences are still present which can affect the spectral parameters of an extended source positioned off-axis like Abell 3783 in the present observation. In the 2.5-arcmin aperture, the fit to the individual MOS1 data returns $kT = 5.42^{+0.54}_{-0.41}$, $Z = 0.59^{+0.20}_{-0.18}$ and XSPEC norm $= 1.98 \pm 0.11 \times 10^{-3}$ (χ^2/d.o.f. $= 111/105$); for MOS 2 $kT = 4.44^{+0.44}_{-0.39}$, $Z = 0.24^{+0.15}_{-0.14}$ and norm $= 1.93 \pm 0.10 \times 10^{-3}$ (χ^2/d.o.f. $= 96/114$); for pn $kT = 4.54^{+0.40}_{-0.36}$, $Z = 0.25^{+0.12}_{-0.11}$ and norm $= 1.77 \pm 0.07 \times 10^{-3}$($\chi^2$/d.o.f. $= 176/186$). The above results correspond to an unabsorbed flux in the 0.5–2 keV band of $8.91 \pm 0.70 \times 10^{-13}$ erg cm^{-2} s^{-1} and $L_{500} = (4.38 \pm 0.47) \times 10^{44}$ erg s^{-1} for MOS1, $8.09 \pm 0.60 \times 10^{-13}$ erg cm^{-2} s^{-1} and $L_{500} = (3.49 \pm 0.36) \times 10^{44}$ erg s^{-1} for MOS2, $7.40 \pm 0.48 \times 10^{-13}$ erg cm^{-2} s^{-1} and $L_{500} = (3.22 \pm 0.31) \times 10^{44}$ erg s^{-1} for pn. The results are within 1σ of the best joint fit and the overall trend of higher fluxes of the MOS compared to the pn is consistent with the current calibration uncertainties (Guainazzi 2008; Mateos et al. 2009).

Radial range used in the surface brightness fitting. Simulations and simple analytic models pointed out how the β model overestimates gas mass because it returns a biased low β due to the restricted range of radii where the fit is performed (e.g. Bartelmann & Steinmetz 1996; Roncarelli et al. 2006). Indeed, recent analyses investigating surface brightness profiles of clusters with *ROSAT* and *Chandra* find evidence for a steepening of the gas density slope with

radius for clusters (Vikhlinin et al. 1999, 2006; Ettori & Balestra 2009). We investigated fitting the surface brightness profile in a narrower range (5 arcmin) and wider range (9 arcmin) compared to the choice made in the analysis. Using the narrower range, we obtain a core radius of $r_c = 90 \pm 16$ kpc (28 ± 5 arcsec) and $\beta = 0.46 \pm 0.03$ for a χ^2/d.o.f. $= 149/129$ and using the wider range we obtain $r_c = 162 \pm 16$ kpc (50 ± 5 arcsec) and $\beta = 0.65 \pm 0.04$ for a χ^2/d.o.f. $= 338/156$. The use of a radial range as large as possible is clearly preferred in the determination of the β-model parameters, but we did not adopt the fit obtained in the 9-arcmin aperture because of the large residuals due to a not optimal fitting of the background level. This is due to the fact that, because of the off-axis position of the source, the increased radial range is obtained with only a partial azimuthal coverage due to the increasing out of field-of-view area (only ~40 per cent of the 6–9 arcmin annulus is covered by data in the MOS1 and pn detectors). Had we used the parameters obtained in the narrower range, we would have derived $M_{500} = (2.13 \pm 0.27) \times 10^{14}$ M$_\odot$ within $r_{500} = 851 \pm 36$ kpc and $M_{vir} = (4.45 \pm 0.56) \times 10^{14}$ M$_\odot$, within the virial radius $r_{vir} = 1765 \pm 73$ kpc, whereas using the wider range, we would have derived $M_{500} = (3.50 \pm 0.43) \times 10^{14}$ M$_\odot$ within $r_{500} = 1005 \pm 41$ kpc and $M_{vir} = (7.44 \pm 0.90) \times 10^{14}$ M$_\odot$, within the virial radius $r_{vir} = 2095 \pm 84$ kpc.

This paper has been typeset from a T$_E$X/L^{A}T$_E$X file prepared by the author.